Available online at www.sciencedirect.com

ScienceDirect

Mendeleev Commun., 2024, **34**, 637–639

Mendeleev Communications

Dual contrasting ability of $NaGd_{0.7}Eu_{0.3}F_4$ nanocrystals tuned by their hydrophilic coating mode

Alexey A. Dovzhenko,[a] Anna A. Betina,[b] Tatyana S. Bulatova,[b] Nikita A. Bogachev,[b] Vladimir G. Nikiforov,[c] Alexandra D. Voloshina,[a] Rustem R. Zairov,[a,d] Asya R. Mustafina,[a] Andrey S. Mereshchenko*[b] and Bulat S. Akhmadeev*[a,d]

[a] *A. E. Arbuzov Institute of Organic and Physical Chemistry, FRC Kazan Scientific Center of the Russian Academy of Sciences, 420088 Kazan, Russian Federation. E-mail: bulat_ahmadeev@mail.ru*

[b] *Department of Laser Chemistry and Laser Materials Science, Institute of Chemistry, St. Petersburg State University, 199034 St. Petersburg, Russian Federation. E-mail: a.mereshchenko@spbu.ru*

[c] *E. K. Zavoisky Physical-Technical Institute, Kazan Scientific Center of the Russian Academy of Sciences, 420029 Kazan, Russian Federation*

[d] *A. M. Butlerov Institute of Chemistry, Kazan Federal University, 420008 Kazan, Russian Federation*

DOI: 10.1016/j.mencom.2024.09.004

This work introduces non-covalent hydrophilic coating of $NaGd_{0.7}Eu_{0.3}F_4$ nanocrystals by polylysine (PL) and polyethyleneimine (PEI) for MRI and fluorescent imaging purposes. PL- and PEI-stabilized nanocrystals exhibit high colloidal stability, cell internalization, fluorescent contrasting of nuclei and cytoplasm, low cytotoxicity, and relaxivity (r_1 = 0.17 dm^3 mmol^{-1} s^{-1} and r_1 = 0.23 dm^3 mmol^{-1} s^{-1}).

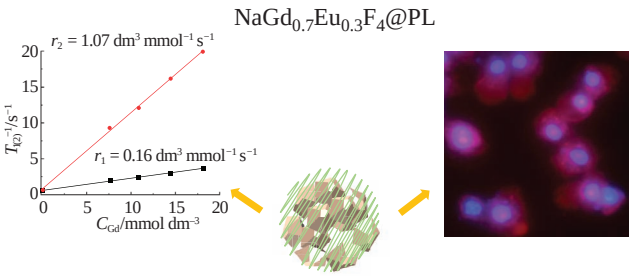

Keywords: contrast agent, hydrophilic coating, fluoride nanoparticle, cell internalization, fluorescent imaging, polymer, Eu-based luminescence.

The relentless interest in fluoride nanoparticles in last decades is due to the wide possibilities of varying their functional properties by introducing various lanthanides.[1] This makes it possible to control the size of nanoparticles[2] and their magnetic[3] and luminescent properties,[4] which ultimately leads to the control of the spectral range[5] and the creation of an up-conversion system[6] and multimodal nanoparticles.[7] In turn, the hydrophilic coating of nanoparticles is needed to increase their colloidal stability and *in vivo* applicability.[8] As a rule, the hydrophilic coating is represented by surfactants,[9] polymers,[10] lipids,[11] *etc*. This allows one to achieve low toxicity[12] by increasing passive targeting to different tumors.[12,13]

In accordance with the previously published works,[14–16] the $NaGd_{0.7}Eu_{0.3}F_4$ nanoparticles (d_{av} = 42 nm) were synthesized, aiming to their Eu^{3+}-based red luminescent and Gd^{3+}-based paramagnetic properties and the smallest size, which may facilitate higher relaxivity[17] and effective penetration into cells and tissues. The low electrokinetic potential of $NaGd_{0.7}Eu_{0.3}F_4$ nanoparticles (−7 ± 2 mV) leads to colloidal instability and formation of large aggregates in water and blood plasma simulating solution [Figure 1(*a*)]. It was a prerequisite for their further hydrophilization by polyethyleneimine (PEI) and poly-DL-lysine (PL) coatings. The excess quantity of PEI and PL was removed from the $NaGd_{0.7}Eu_{0.3}F_4$ nanoparticles coated with PL and PEI by centrifugation, since high levels of PEI and PL can cause additional cytotoxicity.[18] The concentrations of the polymers required for colloid stabilization of NPs@PL and NPs@PEI were determined (see Online Supplementary Materials). It was shown that the colloidal stabilization of NPs@PL and NPs@PEI at a concentration of 26.5 mmol dm^{-3} is eventually provided by 0.0276 mM and 0.0224 mM solutions of PEI and PL, respectively. Such low concentrations are sufficient to stabilize nanoparticles.

Hereinafter, $NaGd_{0.7}Eu_{0.3}F_4$ coated by PL and PEI will be designated as NPs@PL and NPs@PEI, respectively. The resulting nanoparticles have an average size of ~170 nm and a polydispersity index PdI < 0.2 [Figure 1(*a*)]. Strong ionic background (Tris buffer solution) leads to a slight increase in the particle size [Figure 1(*a*)]. At the same time, a noncritical increase in the particle size is observed in BSA solutions (1 g dm^{-3}) at pH 7.4. This indicates high colloidal stability achieved through non-covalent coating of nanoparticles with PEI and PL polymers.

The longitudinal (r_1) and transverse (r_2) relaxivities are used for quantitative evaluation of the MR-contrasting ability.[17] The r_1 and r_2 values are calculated as the relaxation rates $T_{1(2)}^{-1}$ (in s^{-1}) per 1 mmol dm^{-3} of Gd^{III} under the subtraction of T_{diam}^{-1}, which is the relaxation rate of pure water according to the equation: $T_{1(2)}^{-1} = r_{1(2)} \times C_{Gd} + T_{diam}^{-1}$. Linearity of the dependences of $T_{1(2)}^{-1}$ on concentration allowed the relaxivity $r_{1(2)}$ to be calculated. The obtained values are r_1 = 0.23 dm^3 mmol^{-1} s^{-1} and r_2 = = 1.06 dm^3 mmol^{-1} s^{-1} for NPs@PL and r_1 = 0.16 dm^3 mmol^{-1} s^{-1} and r_2=1.07 dm^3 mmol^{-1} s^{-1} for NPs@PEI at 20 MHz and 298 K [Fgiures 1(*b*,*c*)]. These values are much smaller than those for the commercially available contrast agents such as Omniscan, Gadovist, *etc*.,[19] and the nature of hydrophilic coating slightly influences the relaxivity values [Figures 1(*b*,*c*)]. It is worth noting that the agglomeration of lanthanide-based nanoparticles

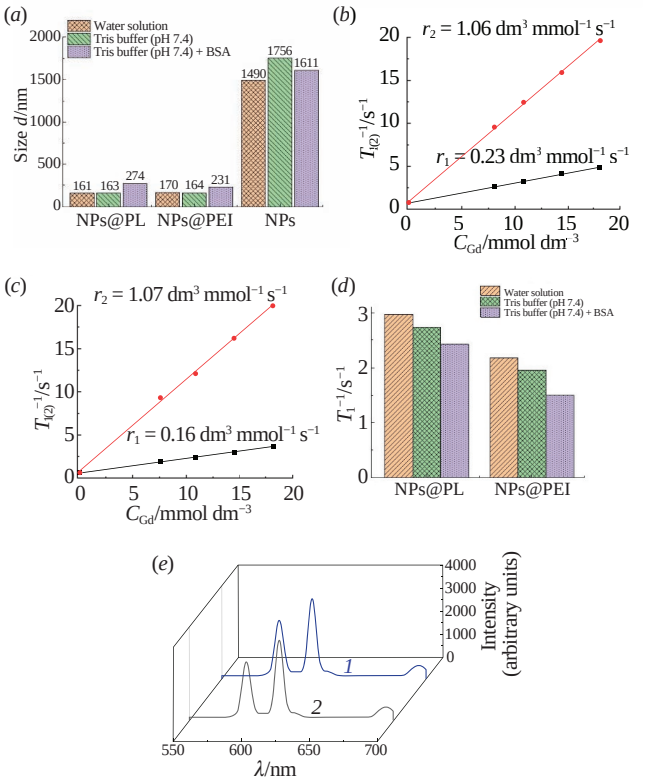

Figure 1 (*a*) Size of NPs, NPs@PL and NPs@PEI in water, Tris buffer, and Tris buffer with BSA media; $T_{1(2)}^{-1}$ *vs* Gd concentration obtained for (*b*) NPs@PL and (*c*) NPs@PEI; (*d*) T_1^{-1} values measured for NPs@PEI and NPs@PL in different solutions; (*e*) luminescence spectra of (*1*) NPs@PL and (*2*) NPs@PEI.

is a very common reason for the low relaxivity values, since hydration of the interfacial Gd^{III} ions is restricted by the agglomeration of such nanoparticles.[20] The average sizes revealed for NPs@PL and NPs@PEI in aqueous solutions [Figure 1(*a*)] confirm that the agglomeration is the reason for the low relaxivity values [Figures 1(*b*,*c*)].

Measurements of the relaxation rate of NPs@PL and NPs@PEI in solutions simulating blood composition showed a slight decrease in the T_1^{-1} values [Figure 1(*d*)], which can be associated with the changes in their aggregation behavior in these media [Figure 1(*a*)].

Eu-based red luminescence of NPs@PL and NPs@PEI [Figure 1(*e*)] makes it possible to use them as an intracellular visualizer. The intensity of the dipole transition $^5D_0 \rightarrow {}^7F_2$ sensitive to local symmetry and strength of the ligand field around Eu^{3+} ions are close to that of the magnetic dipole transition $^5D_0 \rightarrow {}^7F_1$ insensitive to the changes in the surrounding charge distribution, which is typical for Eu^{3+} inorganic salts and oxides with high local symmetry of the Eu^{3+} environment.[21]

The cytotoxic effect of NPs@PL and NPs@PEI was evaluated by measuring the cell viability of M-Hela and Chang liver cell lines after incubation in solutions with different concentrations of the nanoparticles. The half-maximal inhibitory concentration (IC_{50}) values are above 1.7 g dm^{-3} for NPs@PL and NPs@PEI (Table S3). However, the cytotoxicity of NPs@PEI is greater compared to that of NPs@PL, which can be associated with the greater cytotoxicity of PEI constituting the exterior layer.

Flow cytometry measurements were performed for evaluation and comparison of the cellular uptake of NPs@PL and NPs@PEI by M-HeLa cancer cells (Figure S3). A significant increase in red fluorescence was observed after 24 h of incubation of M-Hela cells with NPs@PL and NPs@PEI. It is indicative of the penetration of NPs@PL and NPs@PEI into cells. It is worth noting that NPs@PL (Figure S2) shows higher internalization than NPs@PEI. Further visualization of intracellular internalization of NPs@PEI and NPs@PL was achieved by fluorescence

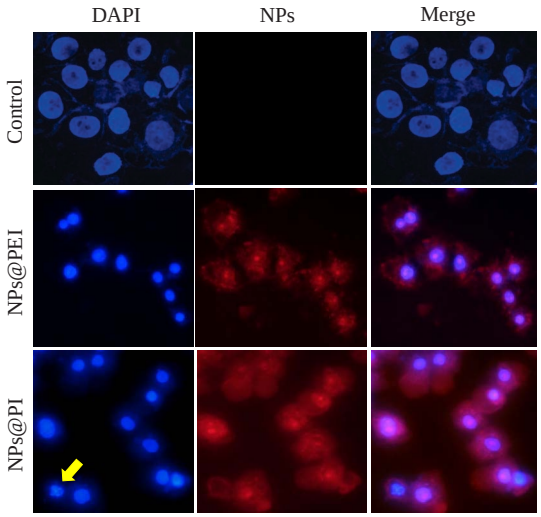

Figure 2 Fluorescence microscopy analysis of the absorption of NPs@PEI and NPs@PL test systems by M-HeLa cells (yellow arrow indicates the morphological changes of the nucleus).

microscopy imaging. In particular, both types of nanoparticles penetrated into M-Hela cancer cells and evenly distributed in the cytoplasm and nuclei. In accordance with flow cytometry, permeation of NPs@PL into cells and nuclei is more effective. Analysis of the morphology of M-HeLa cells after incubation with 4′,6-diamidino-2-phenylindole (DAPI) and NPs@PL and NPs@PEI revealed an obvious nuclear damage compared to the control (Figure 2). A significant decrease in the nuclei size and the formation of a round shape were identified. Moreover, typical signs of apoptosis were observed: the presence of apoptotic bodies, characterized by the preservation of the cell membrane and the bright blue glow of fragmented DNA (Figure 2). The reasons for these processes and the therapeutic utility of NPs@PEI and NPs@PL are subject to the future work.

Thus, this work presents two colloidal systems based on $NaGd_{0.7}Eu_{0.3}F_4$ nanoparticles with low cytotoxicity (IC_{50} > > 1.7 g dm^{-3}) and red luminescent properties. It has been shown that coating of $NaGd_{0.7}Eu_{0.3}F_4$ NPs by PL and PEI provides colloidal stability in water and blood simulating aqueous solution. The optimal hydrophilic coating of NPs@PL and NPs@PEI provides their low cytotoxicity and efficient cellular uptake behavior. The more efficient fluorescent contrasting of the cancer cells by $NaGd_{0.7}Eu_{0.3}F_4$ nanoparticles stabilized with polylysine compared to those stabilized with polyethyleneimines is derived from the greater uptake of the former. This demonstrates one more advantage of polylysine *vs* polyethyleneimine molecules as building blocks of the hydrophilic coating. The fact that NPs@PL exhibit lower cytotoxicity compared with NPs@PEI is another advantage of the hydrophilic coating constructed from PL molecules.

Nanoparticles $NaGd_{0.7}Eu_{0.3}F_4$ were synthesized in the framework of the project funded by The Fellowship of the President of Russia MD-1191.2022.1.3 (PI A. S. Mereshchenko). The study of colloidal and biological properties was carried out as a part of the state assignment of FRC Kazan Scientific Center of RAS. NMR relaxation measurements were supported by the Strategic Academic Leadership Program (PRIORITY-2030) of Kazan Federal University, Russia. The authors are grateful for financial support from the government assignment for FRC Kazan Scientific Center of RAS.

Online Supplementary Materials

Supplementary data associated with this article can be found in the online version at doi: 10.1016/j.mencom.2024.09.004.

References

1 Y. Min, X. Ding, B. Yu, Y. Shen and H. Cong, *Mater. Today Chem.*, 2023, **27**, 101335.
2 N. J. J. Johnson, W. Oakden, G. J. Stanisz, R. S. Prosser and F. C. J. M. van Veggel, *Chem. Mater.*, 2011, **23**, 3714.
3 S. Yamini, M. Gunaseelan, G. A. Kumar, S. Singh, G. C. Dannangoda, K. S. Martirosyan, D. K. Sardar, S. Sivakumar, A. Girigoswami and J. Senthilselvan, *Microchim. Acta*, 2020, **187**, 317.
4 R. Xu, H. Cao, D. Lin, B. Yu and J. Qu, *Cell Rep. Phys. Sci.*, 2022, **3**, 100922.
5 Q. Wu, J. Pei and G. De, *J. Lumin.*, 2014, **152**, 192.
6 H. Yang, A. Zhang, H. Guo, D. Li, S. Xu and L. Lei, *J. Mater. Chem. C*, 2023, **11**, 12915.
7 S. Biju, J. Gallo, M. Bañobre-López, B. B. Manshian, S. J. Soenen, U. Himmelreich, L. V. Elst and T. N. Parac-Vogt, *Chem. – Eur. J.*, 2018, **24**, 7388.
8 B. S. Akhmadeev, I. R. Nizameev, K. V. Kholin, A. D. Voloshina, T. P. Gerasimova, A. T. Gubaidullin, M. K. Kadirov, I. E. Ismaev, K. A. Brylev, R. R. Zairov and A. R. Mustafina, *Pharmaceutics*, 2022, **14**, 1508.
9 F. He, N. Niu, L. Wang, J. Xu, Y. Wang, G. Yang, S. Gai and P. Yang, *Dalton Trans.*, 2013, **42**, 10019.
10 E. Wysokińska, J. Cichos, E. Zioło, A. Bednarkiewicz, L. Strządała, M. Karbowiak, D. Hreniak and W. Kałas, *Toxicol. In Vitro*, 2016, **32**, 16.
11 Y. Huang, E. Hemmer, F. Rosei and F. Vetrone, *J. Phys. Chem. B*, 2016, **120**, 4992.
12 Y. Yan, L. Ding, L. Liu, M. M. A. Abualrejal, H. Chen and Z. Wang, *RSC Adv.*, 2020, **10**, 13872.
13 E. N. M. Cheung, R. D. A. Alvares, W. Oakden, R. Chaudhary, M. L. Hill, J. Pichaandi, G. C. H. Mo, C. Yip, P. M. Macdonald, G. J. Stanisz, F. C. J. M. van Veggel and R. S. Prosser, *Chem. Mater.*, 2010, **22**, 4728.
14 I. E. Kolesnikov, A. A. Vidyakina, M. S. Vasileva, V. G. Nosov, N. A. Bogachev, V. B. Sosnovsky, M. Y. Skripkin, I. I. Tumkin, E. Lähderanta and A. S. Mereshchenko, *New J. Chem.*, 2021, **45**, 10599.
15 T. S. Bulatova, N. A. Bogachev, A. A. Betina, A. N. Smirnov, E. V. Solovieva, M. Yu. Skripkin and A. S. Mereshchenko, *Russ. J. Gen. Chem.*, 2022, **92**, 2845.
16 N. A. Bogachev, A. A. Betina, T. S. Bulatova, V. G. Nosov, S. S. Kolesnik, I. I. Tumkin, M. N. Ryazantsev, M. Yu. Skripkin and A. S. Mereshchenko, *Nanomaterials*, 2022, **12**, 2972.
17 P. Caravan and Z. Zhang, *Eur. J. Inorg. Chem.*, 2012, 1916.
18 C. Brunot, L. Ponsonnet, C. Lagneau, P. Farge, C. Picart and B. Grosgogeat, *Biomaterials*, 2007, **28**, 632.
19 P. Caravan, J. J. Ellison, T. J. McMurry and R. B. Lauffer, *Chem. Rev.*, 1999, **99**, 2293.
20 M. Ahrén, L. Selegård, A. Klasson, F. Söderlind, N. Abrikossova, C. Skoglund, T. Bengtsson, M. Engström, P.-O. Käll and K. Uvdal, *Langmuir*, 2010, **26**, 5753.
21 D. Levy, R. Reisfeld and D. Avnir, *Chem. Phys. Lett.*, 1984, **109**, 593.

Received: 19th March 2024; Com. 24/7427